

Synthesis and thermal characterization of the C-S-H/paraffin composite phase change material utilizing a discontinuous two-step nucleation method

Shen Xuyan¹ Feng Pan^{1,2} Zhang Qi¹

(¹School of Materials Science and Engineering, Southeast University, Nanjing 211189, China)
(²State Key Laboratory of High Performance Civil Engineering Materials, Nanjing 210008, China)

Abstract: The novel calcium-silicate-hydrate (C-S-H)/paraffin composite phase change materials were synthesized using a discontinuous two-step nucleation method. Initially, the C-S-H precursor is separated and dried, followed by immersion in an aqueous environment to transform it into C-S-H. This two-step nucleation approach results in C-S-H with a specific surface area of 497.2 m²/g, achieved by preventing C-S-H foil overlapping and refining its pore structure. When impregnated with paraffin, the novel C-S-H/paraffin composite exhibits superior thermal properties, such as a higher potential heat value of 148.3 J/g and an encapsulation efficiency of 81.6%, outperforming conventional C-S-H. Moreover, the composite material demonstrates excellent cyclic performance, indicating its potential for building thermal storage compared to other paraffin-based composites. Compared with the conventional method, this simple technology, which only adds conversion and centrifugation steps, does not negatively impact preparation costs, the environment, and resource consumption. This study provides valuable theoretical insights for designing thermal storage concrete materials and advancing building heat management.

Key words: two-step nucleation; C-S-H; paraffin; phase change materials; composite; building thermal management

DOI:10.3969/j.issn.1003-7985.2024.04.001

Heat management is a crucial element of modern energy systems, with efficient heat storage and utilization becoming key focuses in construction and energy fields^[1]. Phase change materials (PCMs) offer the ability to store and release significant amounts of energy during phase transitions while maintaining nearly constant temperature. The excellent performance of PCMs renders

them highly attractive in thermal management technologies, potentially aiding in achieving carbon peak and carbon neutrality goals.

PCMs have been successfully applied in construction. One approach involves directly incorporating PCMs into concrete to stabilize indoor temperatures, reducing internal maintenance energy consumption and enhancing the heat management performance of the buildings. For instance, Cabeza et al.^[2] added Micronal © PCM (melting point of 26 °C) produced by BASF into concrete walls. They measured temperature variations in various wall orientations under different conditions, such as window openings, and found that rooms with PCMs experienced a maximum temperature reduction of 3 °C. A major hindrance to the wide application of PCMs is the leakage that occurs owing to their repetitive phase changes. Therefore, PCMs are often incorporated into porous supporting materials to enhance their stability. These composite PCMs are also applied in construction. Shen et al.^[3] used crushed lightweight shale to adsorb paraffin, which was then substituted for coarse aggregates in concrete. At a dosage of 6%, the average specific heat capacity of the phase change concrete increased by 41.23%. Erdogmus et al.^[4] incorporated methyl palmitate PCMs into sludge treated with vacuum impregnation and then added this composite PCM into foam concrete. Compared to the control group without PCMs, this phase change concrete maintained lower indoor temperatures for up to 8 h during high solar intensity, achieving a maximum temperature difference reaching -3 °C.

During the complexation and encapsulation of PCMs, porous minerals like expanded perlite and diatomaceous earth are often selected as supporting materials. Calcium-silicate-hydrate (C-S-H), an inorganic porous material similar to clay minerals, is the most abundant product in cement hydration^[5-6]. C-S-H has a widespread presence owing to extensive cement use. Compared to natural minerals, using C-S-H as a supporting material for PCMs is environmentally and resource-efficient. Furthermore, phase change composites prepared with C-S-H, a key component of cement, exhibit excellent compatibility with cement, theoretically minimizing the negative impact of impurities on cement hydration and strength. The

Received 2024-03-02, **Revised** 2024-05-25.

Biographies: Shen Xuyan (1997—), male, Ph. D. candidate; Feng Pan (corresponding author), female, doctor, professor, pan.feng@seu.edu.cn.

Foundation items: The National Natural Science Foundation of China (No. 52122802, 52078126), Jiangsu Provincial Department of Science and Technology Innovation Support Program (No. BK20222004, BZ2022036).

Citation: Shen Xuyan, Feng Pan, Zhang Qi. Synthesis and thermal characterization of the C-S-H/paraffin composite phase change material utilizing a discontinuous two-step nucleation method [J]. Journal of Southeast University (English Edition), 2024, 40(4): 327–335. DOI: 10.3969/j.issn.1003-7985.2024.04.001.

nano-layered structure of C-S-H provides abundant pores for PCM impregnation, and its high specific surface area (SSA) makes it an ideal supporting material. Jiang et al.^[7] impregnated lauric acid (LA) into C-S-H to create a C-S-H/LA phase change composite with a latent heat value of 32.04 J/g. Subsequently, Shamsaei et al.^[8] designed a “sandwich” structure by growing C-S-H on a graphene oxide (GO) substrate, resulting in a C-S-H/GO composite with an ultra-large SSA of 677 m²/g. The latent heat of the LA phase change composite increased to 127.6 J/g using the prepared C-S-H/GO. Therefore, it is crucial for PCMs based on C-S-H to increase the specific surface and pore structure of C-S-H.

In recent years, C-S-H has been observed to undergo a two-step nucleation process, where precursor formation precedes its transformation into the final C-S-H^[9–10]. The presence of these precursors provides a potential way to control the formation of inorganic materials, allowing for modifications in the properties of the final product by intervening in this nucleation process. For example, the aggregation and crystallization processes of calcium carbonate precursors can be delayed using triethylamine (TEA) to block the terminal carbonate group. The precursor is then concentrated by centrifugation, and TEA is removed, leading to re-aggregation and crystallization. Ultimately, the mechanical and optical properties of the prepared calcium carbonate were comparable to those of single-crystal calcite^[11].

Inspired by this approach, a novel discontinuous two-step nucleation method is proposed to prepare C-S-H in this study. Specifically, the C-S-H precursor is separated from the synthesized solution, dried, and then immersed in an aqueous environment to complete the transformation. This non-continuous two-step nucleation method significantly enhances the SSA while increasing and thinning the pores. The prepared C-S-H is then impregnated with paraffin to form a phase change composite with a

latent heat value of 144.3 J/g (up to 81.6% of pure paraffin used). Compared to other methods investigated for phase change composites of C-S-H, this study features a simpler preparation method and more effective control over pore structure and SSA. Ultimately, the C-S-H/paraffin composite exhibits higher encapsulation efficiency and latent heat than other paraffin-based phase change composites. This study provides theoretical guidance for developing phase change concrete and advancements in building heat management.

1 Materials and Methods

1.1 Materials

Calcium nitrate tetrahydrate ($\text{Ca}(\text{NO}_3)_2 \cdot 4\text{H}_2\text{O}$, AR), isopropanol (AR), and paraffin with melting point of 50–52 °C were purchased from Sinopharm Chemical Reagent Co., Ltd. Sodium metasilicate pentahydrate ($\text{Na}_2\text{SiO}_3 \cdot 5\text{H}_2\text{O}$, AR) was purchased from Shanghai Macklin Biochemical Co., Ltd. All the chemicals were used without any further processing.

1.2 Preparations

1.2.1 Preparation of the C-S-H based on discontinuous two-step nucleation

The preparation process is illustrated in Fig. 1. First, 1.0607 g of $\text{Na}_2\text{SiO}_3 \cdot 5\text{H}_2\text{O}$ and 1.1807 g $\text{Ca}(\text{NO}_3)_2 \cdot 4\text{H}_2\text{O}$ were each dissolved into 100 mL of ultrapure water with vigorous magnetic stirring. The solutions were then mixed within 2 s in a polytetrafluoroethylene (PTFE) beaker, resulting in the immediate formation of a white precipitate. After stirring magnetically for 1 min, vacuum filtration was performed to separate the solid from the liquid, using a Buchner funnel equipped with a mixed cellulose ester (MCE) filter membrane with a pore size of 450 μm. The solid was washed three times with ultrapure water, followed by three washes with isopropanol to

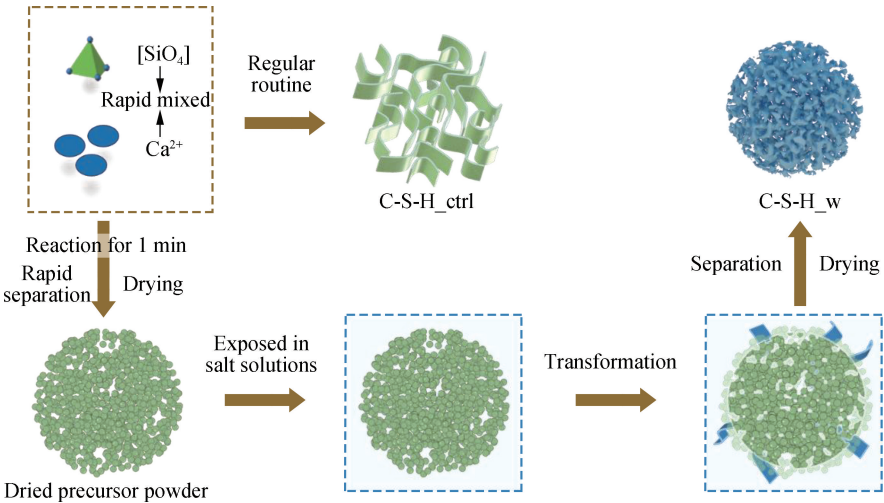


Fig. 1 Schematic representations for the preparation

obtain C-S-H precursor wet gel. The wet gel was then immersed in excess isopropanol for 24 h, followed by centrifugation to collect the solid. The obtained solid was dried to a constant weight in a vacuum oven at 40 °C to obtain solid C-S-H precursors. This method has been demonstrated to reproducibly prepare C-S-H precursors with a stable calcium-to-silicon ratio (Ca/Si), crystallinity, and silicate chain structure in previous experiments^[12]. Subsequently, 100 mg of C-S-H precursor was immersed in 20 mL of ultrapure water to transform into C-S-H. The suspension was transferred to a glove box filled with N_2 . After 24 h, centrifugation at 8 000 r/min was performed to collect the solid, which was then washed twice with ultrapure water and twice with isopropanol. Finally, the solid was dried to constant weight in a vacuum oven at 40 °C to obtain C-S-H powder, denoted as C-S-H_w.

1.2.2 Preparation of the control group (conventional C-S-H)

The control group of C-S-H was synthesized using a conventional method where the final C-S-H was obtained directly from the solution without drying the precursor. The detailed preparation process is described as follows: 1.060 7 g $\text{Na}_2\text{SiO}_3 \cdot 5\text{H}_2\text{O}$ and 1.180 7 g $\text{Ca}(\text{NO}_3)_2 \cdot 4\text{H}_2\text{O}$ were dissolved into 100 mL of ultrapure water with vigorous magnetic stirring, respectively. The two solutions were then mixed within 2 s in a polytetrafluoroethylene (PTFE) beaker, resulting in the immediate formation of a white precipitate. This mixture was stirred magnetically for 24 h. After stirring, vacuum filtration was performed to separate the solid from the liquid using a Buchner funnel equipped with an MCE filter membrane with a pore size of 450 μm . The solid was washed three times with ultrapure water and then three times with isopropanol to obtain a C-S-H wet gel. The wet gel was immersed in excess isopropanol for 24 h, followed by centrifugation to collect the solid. Ultimately, the obtained solid was dried to constant weight in a vacuum oven at 40 °C to obtain the control group of C-S-H, denoted as C-S-H_ctrl.

1.2.3 Preparation of the C-S-H/paraffin composite

The C-S-H powder and paraffin were mixed at a mass ratio of 1:10 in a glass culture dish. The culture dishes containing C-S-H and paraffin were then placed in an oven and heated to 80 °C under atmospheric pressure. Once the paraffin had completely melted, the oven was vented continuously for 6 h to allow the molten paraffin to impregnate the pores of the C-S-H. Then, the culture dishes were taken out and placed in the atmosphere to let the mixture solidify. Once solidified, the mixture was placed on double-layered qualitative filter paper and reheated to 80 °C in an oven to remove any free paraffin. This process was repeated, changing the filter paper each time

until no paraffin was detected on the filter paper. The resulting C-S-H/paraffin phase change composite was stored in a vacuum desiccator for characterization. For the two types of C-S-H, the prepared phase change composites were denoted as C-S-H_w/paraffin and C-S-H_ctrl/paraffin, respectively.

1.3 Characterizations

1.3.1 Crystallinity and phase composition

The samples were characterized for crystallinity and phase composition using X-ray diffraction (XRD) on a D8 Advance X-ray diffractometer (Bruker) equipped with a $\text{CuK}\alpha$ X-ray source ($\lambda = 1.540 5 \text{ nm}$). The samples were ground to pass through an 80- μm sieve before characterization. The operating voltage and current were set at 35 kV and 30 mA, respectively. Scanning was performed in the 2θ range of 5-70° with a scanning step of 0.02° and a scanning time of 0.15 s per step.

1.3.2 SSA and pore size distribution

The SSA of the dried C-S-H samples was measured using nitrogen adsorption testing. Each sample (100 mg) was tested on an ASAP 2460 instrument (Micromeritics, USA). Before testing, samples were degassed in a vacuum environment at 40 °C for 16 h to remove surface-adsorbed gases. Subsequently, nitrogen adsorption and desorption were conducted at 77 K, and the isotherms were recorded. The SSA was calculated using the multi-point Brunauer-Emmett-Teller (BET) method, while pore size distribution was determined through the Barret-Joyner-Hallenda (BJH) fitting method.

1.3.3 Morphology

The morphology of the samples was observed using a Tecnai G2 20 transmission electron microscope (TEM) (FEI, USA) operating at an acceleration voltage of 200 kV. The prepared samples were diluted in isopropanol and dropped onto a carbon-coated copper grid. After the excess solvent evaporated, the copper grid loaded with the sample was placed on a sample holder for observation.

Scanning electron microscopy (SEM) was performed on a Nova Nano SEM 450. Operating conditions included a voltage of 15 kV and a working distance of 6.8 mm. Before observation, samples were coated with a layer of platinum to prevent charge accumulation.

1.3.4 Chemical bonds

The chemical bonds of the phase change composite were characterized using Fourier-transform infrared spectroscopy (FT-IR). The phase change composite was first mixed with KBr in a mass ratio of 1:100 and ground into a homogeneous blend. The resulting powder was then pressed into pellets under a pressure of 20 MPa for 30 s for FT-IR characterization. Background spectra were recorded to eliminate atmospheric interference. Ultimately, FT-IR spectra were collected using a Nicolet iS10 instrument (Thermo Fisher) with a resolution of 4 cm^{-1} over a

range of 400–4 000 cm^{-1} , with 16 scans averaged.

1.3.5 Thermal property

The latent heat of the phase change composite was analyzed using differential scanning calorimetry (DSC). The analysis was conducted using a NETZSCH DSC 214 instrument under a nitrogen atmosphere. The samples underwent 50 thermal cycles within a temperature range of 0 to 80 $^{\circ}\text{C}$, with a heating rate of 10 $^{\circ}\text{C}/\text{min}$. The encapsulation efficiency E can be calculated by the following expression:

$$E = \frac{\Delta H_{m,c} + \Delta H_{f,c}}{\Delta H_{m,p} + \Delta H_{f,p}} \times 100\% \quad (1)$$

where ΔH denotes the latent heat, while the subscripts m, f, c, and p represent melting, freezing, composite, and paraffin, respectively^[13].

2 Results and Discussion

2.1 Characterizations of C-S-H

2.1.1 Crystallinity and phase composition

The properties of C-S-H directly determine the performance of the phase change composite with paraffin. The crystallinity and phase composition of the two types of C-S-H were characterized using XRD, and the results are shown in Fig. 2(a). Both products exhibit diffraction peaks at 16.4 $^{\circ}$, 29.3 $^{\circ}$, 32.0 $^{\circ}$, and 49.9 $^{\circ}$, corresponding

to the (101), (110), (200), and (020) planes of C-S-H(I), which is consistent with previous literature reports^[14]. This indicates that both products are single-phase C-S-H with a degree of crystallinity. For C-S-H_w prepared by discontinuous two-step nucleation, the XRD spectrum shows characteristic diffraction peaks identical to those of the control group C-S-H_ctrl synthesized using the conventional method. This suggests that the C-S-H precursor retains the ability to transform into C-S-H in water, even though separation and drying were performed in advance. This finding provides a theoretical basis and technical feasibility for regulating C-S-H properties using the discontinuous two-step nucleation approach.

2.1.2 SSA and pore size distribution

The SSA and pore size distribution of C-S-H are closely related to paraffin impregnation. As a nanoporous mineral, the SSA of C-S-H can be influenced by the preparation method, typically falling within the range of 10 to 200 m^2/g ^[7]. The SSA of the synthesized C-S-H was determined through nitrogen adsorption. Using the multi-point model, the SSA of C-S-H_ctrl was found to be 107.2 m^2/g . Interestingly, the SSA of C-S-H_w reached 497.2 m^2/g , exhibiting a 282.8% increase compared to C-S-H_ctrl. This significant enhancement indicates that the discontinuous two-step nucleation method can substantially increase the SSA of C-S-H.

The pore size distribution of the two types of C-S-H was analyzed (see Fig. 2(b)). C-S-H_w exhibited a larger number of small pores, with pore sizes primarily distributed between 8 nm and 20 nm, whereas C-S-H_ctrl predominantly exhibited pore sizes ranging from 20 nm to 50 nm. This observation is consistent with the SSA results, indicating that the increased number of smaller pores contributes to a larger SSA for C-S-H_w. Moreover, the presence of numerous small pores is beneficial for accommodating more phase change material and preventing its leakage in the composite. This creates the possibility to fabricate better phase change supporting materials using the discontinuous two-step nucleation method.

2.1.3 Morphology

Fig. 3 presents SEM images of two types of C-S-H. The C-S-H_ctrl exhibits a petal-like structure formed by C-S-H foil aggregation, consistent with literature reports^[15]. This aggregated structure results in significant overlapping of C-S-H foil surfaces, leading to a large loss of surface area. By contrast, the morphology of C-S-H_w differs from conventional C-S-H, displaying a crosslinked structure with numerous pores. This morphology prevents surface area loss caused by aggregation and exposes more C-S-H solids and pores, which may be related to the pore structure shown in Fig. 2(b). Additionally, the increase in the SSA of C-S-H through a discontinuous two-step nucleation method may be caused by the transformation into C-S-H based on the framework of ag-

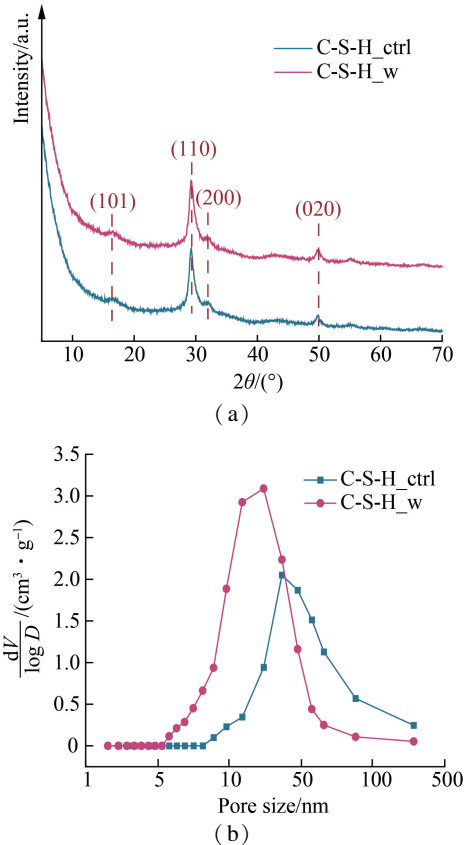


Fig. 2 Characterizations of two kinds of C-S-H. (a) XRD patterns; (b) Pore size distribution

gregated precursor. Specifically, the discontinuous formation of C-S-H was achieved through precursor powder transformation. These powders acted as a solid template, restricting the forming regions of foils and thus influencing the morphology of C-S-H_w to a certain extent. This solid template effectively avoided the agglomeration of C-S-H foils, leading to an increase in the SSA of C-S-H_w (see Fig. 1(d)). However, C-S-H_ctrl formed by homogeneous nucleation in solution, resulting in foils tending to aggregate owing to high surface energy, causing overlap and a reduction in SSA.

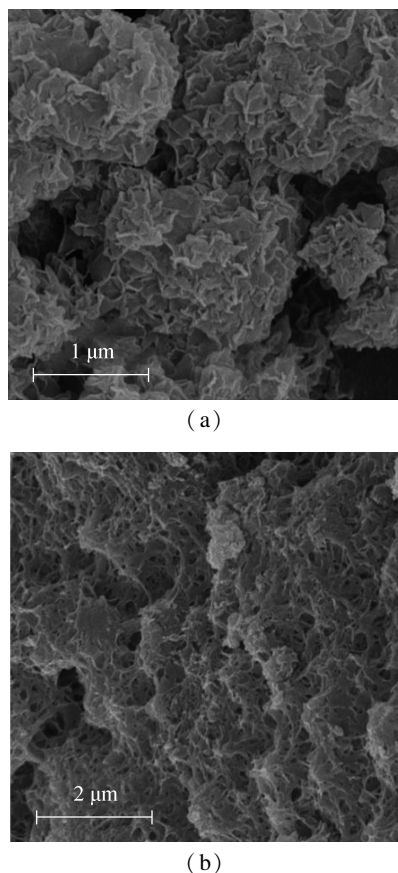


Fig. 3 SEM images. (a) C-S-H_ctrl; (b) C-S-H_w

2.2 C-S-H/paraffin phase change composite

2.2.1 Chemical bonds and pore size distribution

FT-IR was conducted to analyze the interactions between C-S-H and paraffin, as shown in Fig. 4(a). The peaks at 453, 975, and 3 475 cm^{-1} in C-S-H correspond to the deformation of Si-O, the stretching vibration of Si-O (Q^2), and the vibration of O—H in water molecules, respectively. For paraffin, the peaks at 722, 1 378, 1 467, 2 847, and 2 917 cm^{-1} are attributed to the rocking vibration of $-\text{CH}_2$ group, the symmetric and asymmetric bending vibration of CH_3 group, and the symmetric and asymmetric stretching vibration of $-\text{CH}_2$ group, respectively^[16]. The spectra show that both composites display absorption peaks characteristic of C-S-H and paraffin, suggesting compatibility between C-S-H and paraf-

fin. Additionally, a new peak at 1 559 cm^{-1} is observed, which can be attributed to calcium carbonate formed during the composite preparation in the atmosphere^[17].

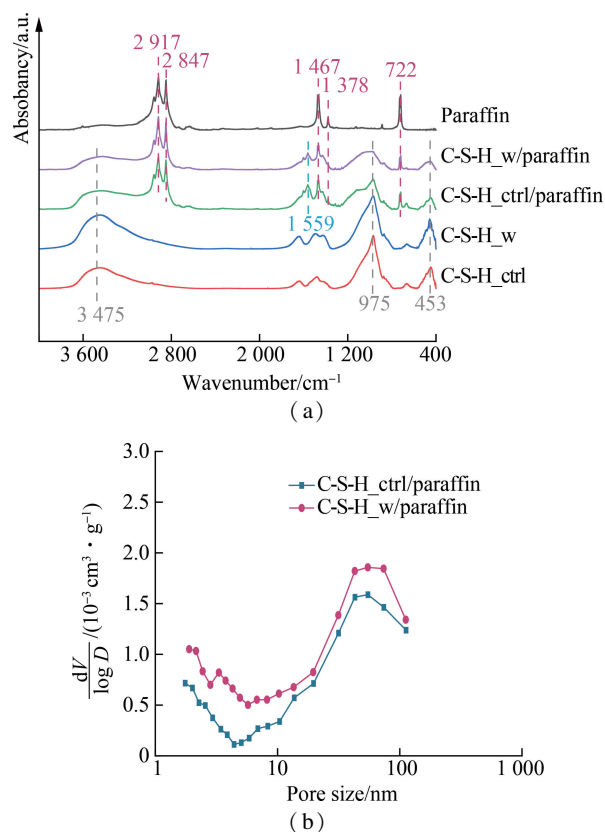


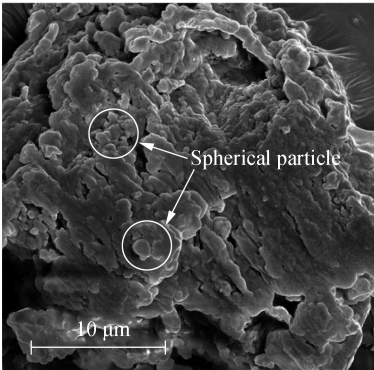
Fig. 4 Complexation of C-S-H and paraffin. (a) FT-IR spectra of the samples; (b) Pore size distribution of the samples

Paraffin impregnation into C-S-H results in a significant decrease in the SSA of the phase change composites compared to pure C-S-H. Specifically, the SSA of the C-S-H_w/paraffin composite is 1.0 m^2/g , while that of the C-S-H_ctrl/paraffin composite is 0.6 m^2/g . Fig. 4(b) illustrates the pore size distribution of the two composites, showing that paraffin impregnation leads to a sharp decrease in the pore volume across various pore sizes to nearly 0. This suggests that paraffin can still be effectively loaded into the C-S-H_w pores, although complete impregnation might be challenging owing to the much smaller pore sizes of C-S-H_w. Combined with FT-IR results, it can be concluded that paraffin is successfully impregnated into the C-S-H pores to form a phase change composite^[7].

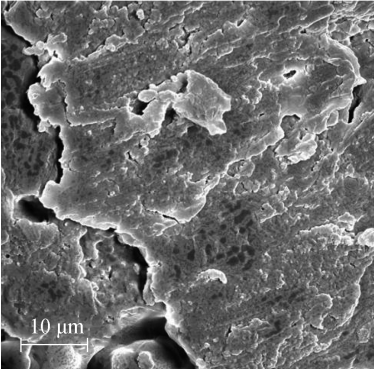
2.2.2 Morphology

SEM was utilized to observe the morphology of the phase change composites. In the C-S-H_ctrl/paraffin composite, the microstructure of the used C-S-H_ctrl consists of 1-2 μm spherical particles formed by the aggregation of C-S-H foils (see Fig. 3(a)). Therefore, after paraffin impregnation, the paraffin wraps around the surface of C-S-H foils, forming spherical particles, as indicated in Fig. 5(a). By contrast, the mixture of paraffin

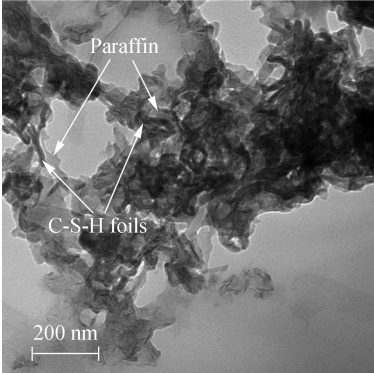
and C-S-H in the C-S-H_w/paraffin composite (see Fig. 5 (b)) is more uniform with a smoother surface, which can be attributed to the crosslinked overall structure of C-S-H_w



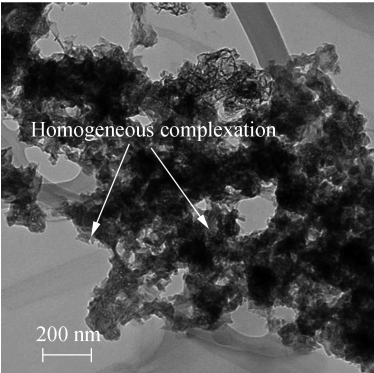
(a)



(b)



(c)



(d)

Fig. 5 SEM and TEM images. (a) SEM image of C-S-H_ctrl; (b) SEM image of C-S-H_w; (c) TEM image of C-S-H_ctrl; (d) TEM image of C-S-H_w

w prepared by discontinuous two-step nucleation. Paraffin is incorporated more thoroughly into the pores of C-S-H_w, enhancing sample uniformity.

The difference is better illustrated by TEM images. As shown in Fig. 5 (c), the C-S-H_ctrl/paraffin composite exhibits distinct phase interfaces between paraffin (the cloudy part with lower contrast) and the C-S-H foils (the skeletal part with higher contrast). However, in the C-S-H_w/paraffin composite, the paraffin distribution is more uniform, with no apparent separation between C-S-H and the impregnated paraffin, as illustrated in Fig. 5 (d). This phenomenon may be attributed to the larger number of pores within C-S-H_w, which facilitates paraffin penetration. The morphology and three-dimensional crosslinked pores of C-S-H_w (see Fig. 3 (b)) also provide favorable evidence for homogeneous paraffin impregnation in the C-S-H_w/paraffin composite.

2.2.3 Thermal properties

Fig. 6(a) presents the DSC curves of pure paraffin and the two composites after 1 thermal cycle. The melting point and freezing point of paraffin are 54.8 and 46.8 °C, respectively. After impregnation into C-S-H_ctrl and C-S-H_w to form composites, the melting points rise to 57.6 and 57.8 °C, while the freezing points decrease to 46.4 and 43.6 °C, respectively. These changes can be attributed to two factors: 1) the delayed effect of heat transfer from the C-S-H matrix to the impregnated paraffin and 2) the supercooling effect caused by the small size of the pores. The latent heat values for the samples are determined by integrating the heat flow over time from the DSC curves, as shown in Table 1. Whether in melting or freezing, pure paraffin exhibits the highest latent heat (approximately 181.7 J/g), which is consistent with values reported by Zhao et al.^[18]. For the two-phase change composites, the latent heat values decrease owing to the C-S-H matrix. The C-S-H_w/paraffin composite, prepared through the discontinuous two-step nucleation method, exhibits a higher latent heat (148.3 J/g) compared to the conventional C-S-H composite (102.8 J/g). Compared to pure paraffin, the encapsulation efficiency of the C-S-H_w/paraffin composite is as high as 81.6%, while that of the C-S-H_ctrl/paraffin composite is only 56.6%. This indicates that the discontinuous two-step nucleation method effectively enhances the performance of C-S-H as a PCM-supporting material. As mentioned above, this enhancement stems from the greater number and narrower pores of C-S-H_w along with its morphology, which can accommodate more paraffin. Fig. 7 compares various phase change composites^[19–25], revealing that the encapsulation efficiency of conventional C-S-H as a supporting material for paraffin is similar to that of most materials. However, the performance of the C-S-H_w/paraffin composite, prepared by discontinuous two-step nucleation, is notably superior. This indicates the adapta-

bility of C-S-H as a support for PCMs and the effectiveness of this improved preparation strategy.

Additionally, 50 thermal cycles from 0 to 80 °C were employed to test the leakage and stability of the C-S-H/paraffin composites, as depicted in Figs. 6(b) and (c). After 50 cycles, both composites maintained their melting and freezing points, with only a slight decrease in latent

heat. Moreover, there were no obvious differences in the FT-IR spectra of the two composites, indicating identical peaks and frequencies. These results suggest that both types of C-S-H phase change composites exhibit good stability in thermal performance and chemical structure, and the paraffin inside the pores does not leak during thermal cycling^[18–19].

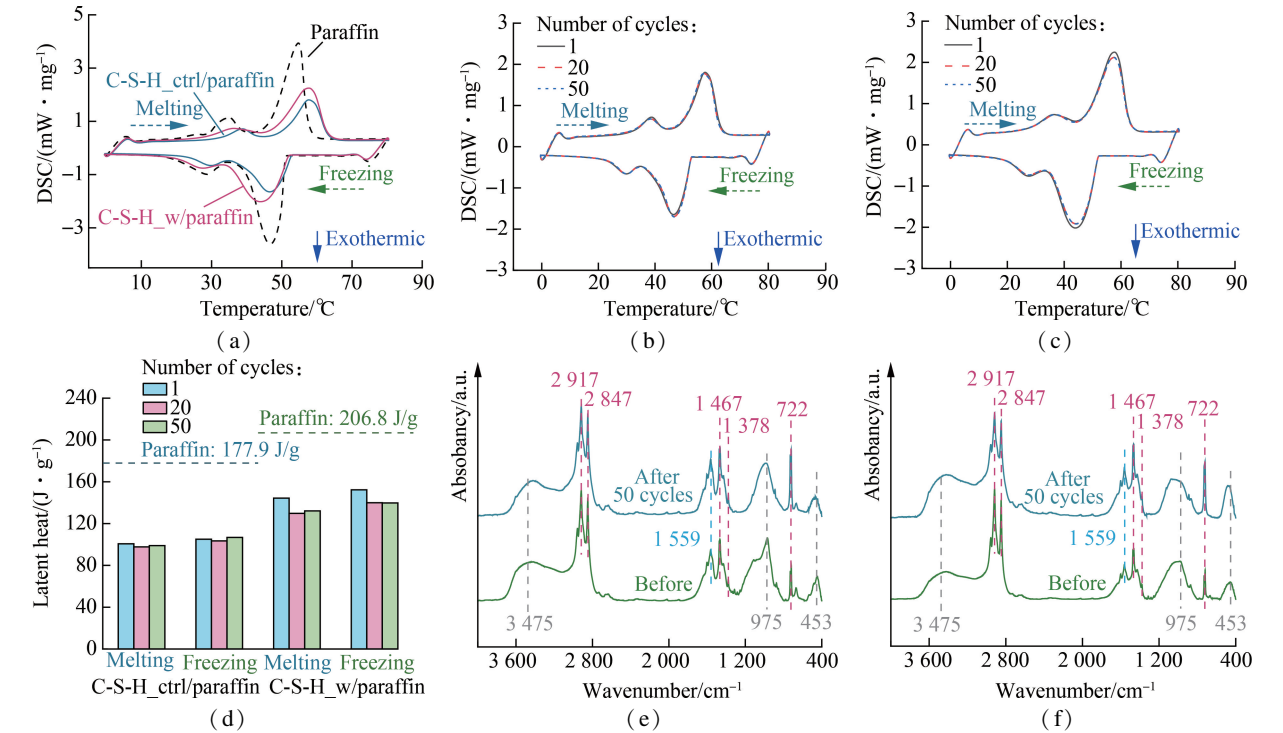


Fig. 6 Performances of thermal storage and stability. (a) DSC curves of the samples after 1 cycle; (b) DSC curves of the C-S-H_ctrl/paraffin composite after 1, 20, and 50 cycles; (c) DSC curves of C-S-H_w/paraffin after 1, 20, and 50 cycles; (d) Latent heat of phase change composites; (e) FT-IR spectra of the C-S-H_ctrl/paraffin composite after 50 cycles; (f) FT-IR spectra of the C-S-H_w/paraffin composite after 50 cycles

Table 1 Phase change temperature and latent heat of the samples

Samples	Melting point/°C	Latent heat of melting/(J · g ⁻¹)	Freezing point/°C	Latent heat of freezing/(J · g ⁻¹)	Average latent heat/(J · g ⁻¹)	Encapsulation efficiency/%
Paraffin	54.8	177.9	46.8	185.5	181.7	100.0
C-S-H_ctrl/paraffin	57.6	100.6	46.4	105.1	102.8	56.6
C-S-H_w/paraffin	57.8	144.3	43.6	152.3	148.3	81.6

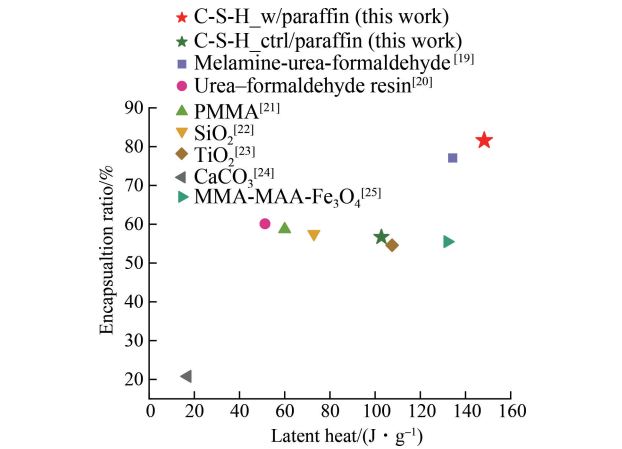


Fig. 7 Comparison of latent heat and encapsulation efficiency of paraffin phase change composites with different supporting materials

3 Conclusions

- 1) The discontinuous two-step nucleation method significantly increased the SSA of C-S-H to 497.2 m²/g. It also enhanced the total pore value and refined the pore structure, making the prepared C-S-H more suitable for paraffin impregnation compared to conventional C-S-H.
- 2) The phase change composite prepared using this method exhibited a latent heat of 148.3 J/g and an encapsulation efficiency of 81.6%, surpassing most current paraffin-based phase change composites.
- 3) C-S-H phase change composites present excellent leakage resistance after 50 thermal cycles from 10 to 80 °C.
- 4) These findings provide important theoretical guidance and practical significance for the application of C-S-H phase change composites in fields such as phase change

concrete and building thermal management.

References

- [1] Fang Y L, Zhang X S, Liu C. Experimental study of lightweight radiant floor heating system with non-full-coverage heat-conducting plate[J]. *Journal of Southeast University (Natural Science Edition)*, 2022, **52** (6): 1104 – 1113. DOI: 10.3969/j.issn.1001-0505.2022.06.010. (in Chinese)
- [2] Cabeza L F, Castellón C, Nogués M, et al. Use of microencapsulated PCM in concrete walls for energy savings [J]. *Energy and Buildings*, 2007, **39** (2): 113 – 119. DOI: 10.1016/j.enbuild.2006.03.030.
- [3] Shen Y L, Liu S L, Zeng C, et al. Experimental thermal study of a new PCM-concrete thermal storage block (PCM-CTSB) [J]. *Construction and Building Materials*, 2021, **293**: 123540. DOI: 10.1016/j.conbuildmat.2021.123540.
- [4] Erdogmus E, Yaras A, Ustaoglu A, et al. Thermal performance analysis of novel foam concrete composites with PCM for energy storage and environmental benefits in buildings [J]. *Energy and Buildings*, 2023, **296**: 113413. DOI: 10.1016/j.enbuild.2023.113413.
- [5] Liu B, Pan G H, Gao M, et al. Influence of grinding aid on the grinding effect of iron tailings and hydration properties of blended cement[J]. *Journal of Southeast University (Natural Science Edition)*, 2022, **52** (5): 907 – 916. DOI: 10.3969/j.issn.1001-0505.2022.05.011. (in Chinese)
- [6] Wang P G, Fu H, Li G G, et al. Effects of Nano-C-S-H-PCE on performance of C50 non-steam cured concrete for coastal subway segment [J]. *Journal of Southeast University (Natural Science Edition)*, 2022, **52** (2): 254 – 262. DOI: 10.3969/j.issn.1001-0505.2022.02.007. (in Chinese)
- [7] Jiang J Y, Zheng Q, Yan Y R, et al. Design of a novel nanocomposite with C-S-H@ LA for thermal energy storage: A theoretical and experimental study [J]. *Applied Energy*, 2018, **220**: 395 – 407. DOI: 10.1016/j.apenergy.2018.03.134.
- [8] Shamsaei E, de Souza F B, Fouladi A, et al. Graphene oxide-based mesoporous calcium silicate hydrate sandwich-like structure: Synthesis and application for thermal energy storage [J]. *ACS Applied Energy Materials*, 2022, **5** (1): 958 – 969. DOI: 10.1021/acsaem.1c03356.
- [9] Shen X Y, Feng P, Zhang Q, et al. Toward the formation mechanism of synthetic calcium silicate hydrate (C-S-H)-pH and kinetic considerations[J]. *Cement and Concrete Research*, 2023, **172**: 107248. DOI: 10.1016/j.cemconres.2023.107248.
- [10] Sowoidnich T, Damidot D, Ludwig H M, et al. The nucleation of C-S-H via prenucleation clusters [J]. *The Journal of Chemical Physics*, 2023, **158** (11): 114309. DOI: 10.1063/5.0141255.
- [11] Liu Z M, Shao C Y, Jin B, et al. Crosslinking ionic oligomers as conformable precursors to calcium carbonate [J]. *Nature*, 2019, **574** (7778): 394 – 398. DOI: 10.1038/s41586-019-1645-x.
- [12] Shen X Y, Feng P, Liu X, et al. New insights into the non-classical nucleation of C-S-H[J]. *Cement and Concrete Research*, 2023, **168**: 107135. DOI: 10.1016/j.cemconres.2023.107135.
- [13] Salunkhe P B, Shembekar P S. A review on effect of phase change material encapsulation on the thermal performance of a system [J]. *Renewable and Sustainable Energy Reviews*, 2012, **16** (8): 5603 – 5616. DOI: 10.1016/j.rser.2012.05.037.
- [14] Matsuyama H, Young J F. Effects of pH on precipitation of quasi-crystalline calcium silicate hydrate in aqueous solution[J]. *Advances in Cement Research*, 2000, **12** (1): 29 – 33. DOI: 10.1680/adcr.2000.12.1.29.
- [15] Liu X, Feng P, Li W, et al. Effects of pH on the nano/micro structure of calcium silicate hydrate (C-S-H) under sulfate attack[J]. *Cement and Concrete Research*, 2021, **140**: 106306. DOI: 10.1016/j.cemconres.2020.106306.
- [16] Wu Y J, Sha S L, Liu H Y, et al. Variable temperature infrared spectroscopy of paraffin[J]. *Measurement Technique*, 2020, **3**: 5 – 10. (in Chinese)
- [17] Niculescu O, Leca M, Moldovan Z, et al. Obtaining and characterization of an ecologic wax emulsions for finishing natural leathers and furs [J]. *Revista De Chimie*, 2015, **66** (8): 1173 – 1176.
- [18] Zhao G, Zhu B D, Zou N N, et al. Research progress of paraffin-based microencapsulated phase change materials [J]. *Polymer Bulletin*, 2023, **36** (9): 1136 – 1146. DOI: 10.14028/j.cnki.1003-3726.2023.09.003. (in Chinese)
- [19] Han S J, Chen Y P, Lü S Y, et al. Effects of processing conditions on the properties of paraffin/melamine-urea-formaldehyde microcapsules prepared by in situ polymerization [J]. *Colloids and Surfaces A: Physicochemical and Engineering Aspects*, 2020, **585**: 124046. DOI: 10.1016/j.colsurfa.2019.124046.
- [20] Huo J H, Peng Z G, Feng Q. Synthesis and properties of microencapsulated phase change material with a urea-formaldehyde resin shell and paraffin wax core [J]. *Journal of Applied Polymer Science*, 2020, **137** (16): e48578. DOI: 10.1002/app.48578.
- [21] Wan X, Zhang H Y, Chen C, et al. Synthesis and characterization of phase change materials microcapsules with paraffin core/cross-linked hybrid polymer shell for thermal energy storage [J]. *Journal of Energy Storage*, 2020, **32**: 101897. DOI: 10.1016/j.est.2020.101897.
- [22] Zhang Q Q, Sun Z C, Li G M, et al. Preparation and printing application of paraffin@ silica phase change microcapsules [J]. *Digital Printing*, 2021, **3**: 85 – 91. DOI: 10.19370/j.cnki.cn10-1304/ts.2021.03.008. (in Chinese)
- [23] Ma X C, Liu Y J, Liu H, et al. Synthesis and characterization of microencapsulated paraffin with TiO₂ shell as thermal energy storage materials [J]. *Journal of Materials Science: Materials in Electronics*, 2018, **29** (17): 15241 – 15248. DOI: 10.1007/s10854-018-9666-z.
- [24] Shi J, Wu X L, Sun R, et al. Synthesis and performance evaluation of paraffin microcapsules with calcium carbonate shell modulated by different anionic surfactants for thermal energy storage [J]. *Colloids and Surfaces A*:

Physicochemical and Engineering Aspects, 2019, **571**: 36–43. DOI: 10.1016/j.colsurfa.2019.03.029.

[25] Zhuang X H, Zhang Y, Cai C, et al. Design the magnetic microencapsulated phase change materials with poly

(MMA-MAA) @ n-octadecane modified by Fe₃O₄ [J]. Scientific Reports, 2018, **8**(1): 16379. DOI: 10.1038/s41598-018-34583-5.

基于非连续两步成核的 C-S-H/paraffin 相变材料制备及储热性能

沈叙言¹ 冯攀^{1,2} 张琪¹

(¹ 东南大学材料科学与工程学院, 南京 211189)
(² 高性能土木工程材料国家重点实验室, 南京 210008)

摘要:通过非连续式的两步成核方法制备了新型 C-S-H/石蜡相变材料,即在前驱体形成后将其分离并干燥,重新置于水中转化为 C-S-H. 由于解决了 C-S-H 箔片的相互遮盖问题以及孔径的大幅细化,通过非连续式两步成核方法制备的 C-S-H 比表面积高达 497.2 m²/g. 与常规方法制备的 C-S-H 相比,在浸渍石蜡后, C-S-H/paraffin 复合材料具有更高的潜热值(148.3 J/g)和更高的封装效率(81.6%),并显示出良好的循环性能. 相比其他石蜡基的相变储能材料,这种新方法制备的 C-S-H 材料在封装效率和潜热值上展现出明显优势. 该方法工艺简单,相比常规方法仅增加了一次转化和离心,成本的提高可以忽略,同时对环境、资源无负面影响. 该研究对相变混凝土、建筑热管理等技术具有理论指导意义.

关键词:两步成核;C-S-H;石蜡;相变材料;复合材料;建筑热管理

中图分类号:TU506